TRITA-FYS 2011:45
ISSN 0280-316X
ISRN KTH/FYS/--11:45—SE

Royal Institute of Technology
School of Engineering Sciences
Nuclear Energy Engineering
Nuclear Power Safety

ANALYSIS OF BOILING WATER REACTOR DESIGN AND OPERATING CONDITIONS EFFECT ON STABILITY BEHAVIOUR

M. Sc. thesis by
Elias AMSELEM

Supervisor:
Dr. Tomasz Kozlowski

Stockholm, Sweden, August 2011

ABSTRACT

It is well known that boiling water reactors can experience inadvertent power oscillations. When such instability occurs the core can oscillate in two different modes (in phase mode and out of phase mode). In the late 90's a stability benchmark was created using the stability data obtained from the experiments at the Swedish nuclear power plant of Ringhals-1. Data was collected from the cycles 14, 15 , 16 and 17. Later on, this data was used to validate the various models and codes with the aim of predicting the instability behavior of the core and understand the triggers of such oscillations. The current trend of increasing reactor power density and relying on natural circulation for core cooling may have consequences for the stability of modern BWR's designs. The objective of this work is to find the most important parameters affecting the stability of the BWRs and propose alternative stability maps. For this purpose a TRACE/PARCS model of the Ringhals-1 NPP will be used. Afterwards a selection of possible parameters and dimensionless numbers will be made to study its effect on stability. Once those parameters are found they will be included in the stability maps to make them more accurate.

PREFACE

This Master's thesis was carried out at the department of Nuclear Power Safety at the Royal Institute of Technology.
I'm grateful to my supervisor Dr. Tomasz Kozlowski for giving me the chance to perform my Master's thesis at KTH, for providing me an interesting and challenging topic and for helping me to fulfill the goals.
I want to thank all the professors for their help and specially the other Nuclear Power Safety master students for their friendship, recommendations and assistance during my stay.
Finally, I would like to express my appreciation and gratitude to my family, especially my parents, for their support, encouragement and advice during my studies and during the realization of this thesis.

August 2011
Elias Amselem

TABLE OF CONTENTS

ABREVIATIONS

BWR: Boiling Water Reactor.
NPP: Nuclear Power Plant.
DWO: Density Wave Oscillation.
DR: Decay Ratio.
NF: Natural Frequency.
APRM: Average Power Range Monitor.
LPRM: Local Power Range Monitor.
NRC: Nuclear Regulatory Commission.
TRACE: TRAC/RELAP Advanced Computational Engine.
PARCS: Purdue Advanced Reactor Core Simulator.
OECD: Organization for Economic Co-operation and Development.
TPC: Total Power Coefficient.
MEOD: Maximum Extended Operating Domain.
APO: Axial Power Offset.

LIST OF TABLES

LIST OF FIGURES

1. INTRODUCTION

1.1 Motivation and objective

Since the beginning of the BWR technology development there was an important concern about nuclear-coupled stability. The first experimental BWRs weren't big enough to present instability and the first commercial BWR were designed in way to avoid instability issues. However, after many years of exploitation, many of those power plants suffered fuel modifications and/or power upgrades. After that, the first indications of stability problems came in the late 70's and during the 80's [1]. Moreover, the actual trend of increasing the reactor power density and to rely on natural circulation for more extensive core cooling will have major repercussion for the stability of advanced BWR designs.[2]

In prevision of the increasing importance of the instability matter inside the new BWR plant design this work pretend to find new tools of understanding and methods that will help to predict and avoid instability related shutdowns. For that purpose thermal hydraulics and neutronics simulation tools will be used to extract real plant data from a NPP model. And this data will be analyzed and used to predict the plant stability behavior.

1.2 BWR Instability issue

1.2.1 Types of Instabilities

In BWRs, thermal power is removed by boiling water in a vertical channel, this may cause instability during the operation due to density changes and thermal-hydraulic feedback mechanisms. Taking into account that the coolant is also a moderator, if the core void content is oscillating it will affect the neutron flux and the power generated. Those, in return, will affect the void fraction. Due to that, inside a BWR we can identify and classify purely thermal-hydraulic instabilities or coupled neutronic-thermal-hydraulic instabilities. [2]

1. Thermal-hydraulic instabilities.

Thermal-hydraulic instabilities can be classified into two categories: static instabilities and dynamic instabilities. The static instabilities found in the reactor are: the flow excursion, the flow pattern relaxation and the geysering. These instabilities follows the steady state laws while the dynamic instabilities follows the dynamic

conservation equations. Some dynamic instabilities are: the density wave oscillation (DWO), the acoustic oscillation and the pressure drop oscillation. From the previous mentioned instabilities, the DWO is the most common one in BWRs. The DWO takes places when, given a flow perturbation, a wave of voids travels upwards through the channel producing a pressure drop that is delayed with respect the original perturbation.

In channel-thermal-hydraulic instability there are two different modes of oscillation: parallel-channel or out-of-phase instabilities and single-channel or in-phase instability. In out-of-phase instability the flow in one channel increase while the flow in other channel decrease. The channel void fraction follows opposite trends to those of the flows while the pressure drop is the same across both channels.[2]

2. Coupled neutronic-thermalhydraulic instabilities.

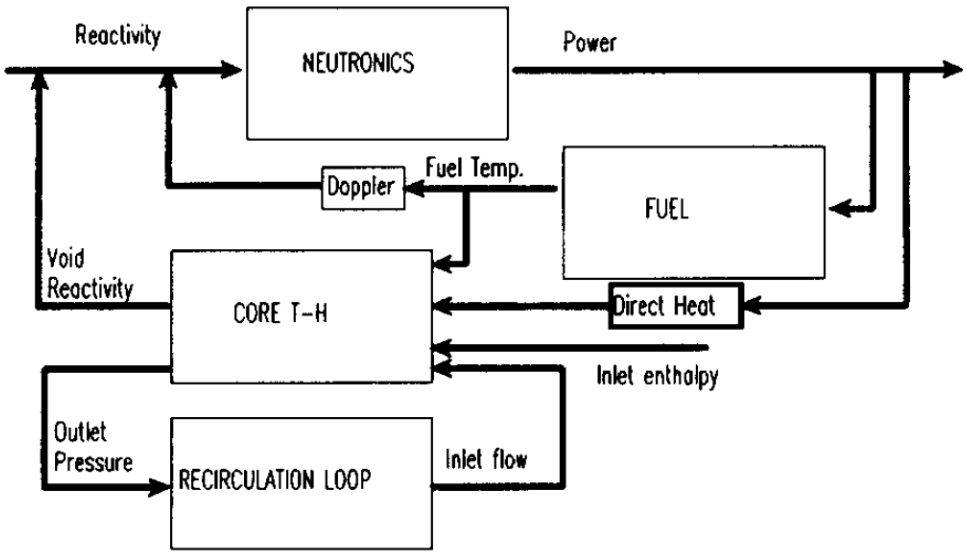

Figure 1. Block diagram for the feedback paths for the coupled neutronics-thermalhydraulics instabilities.[4]

The BWR instabilities are induced by the feedback between the neutronics and the thermal-hydraulics processes. There are four major aspects that affect BWR stability: the core thermal-hydraulics, the neutron kinetics, the fuel dynamics and heat transfer and the ex-core systems. The core thermal-hydraulics act as a trigger for instabilities and directly affects the power production by fission. The neutron kinetics is directly responsible for the power variations. Fuel dynamics and heat transfer works as a filter of power perturbation introducing a time delay (6 to 10 seconds) between power production and coolant flow heating. Finally, the ex-core systems imposes the boundary conditions influencing the stability of core channels. Coupled neutronic-thermal-hydraulic instabilities can be classified in regional or out-of-phase instabilities, when one half of the core oscillates while the other part does the opposite oscillation, and core wide or in-phase instabilities when the power and the inlet flow of the whole core oscillates in phase for all the channels. [2]

1.2.2 Safety relevance.

In terms of safety, during an instability event with high oscillation amplitudes the regarded variables are the neutron flux and the fuel rod surface temperature. Moreover, due to thermal cycling, the fuel rod integrity may be affected because pellet cladding interaction become more probable. In addition, thermal cycling could induce an increase in the fission product release from pellets that can lead to a faster mechanical failure or corrosion of the cladding. Flow oscillations also may cause sustained vibrations of components that could lead to a boiling crisis due to a change in the local heat transfer characteristics.
Nearly thirty planned or unplanned stability events have been reported in BWR (data from 1997). The most noticeable event was the one at LaSalle NPP (USA, Illinois) in 1988. Due to human errors the core reach a condition susceptible of instability and the core power starts to oscillate, finally the reactor automatically scrammed because it reaches high flux, 118% trip. [1]
Even though the plant is not in several danger due to instability issues, the cost of the possible fuel damage and the cost of having unplanned shutdowns remain very high and makes instability in a major problem that needs to be study.

2. METHODOLOGY

The main objective of this work is to do a study on BWR instability and its causes. For that purpose we collect as much relevant data as we can with the aim to find relations between this data and the stability behavior of the plant. This will be done using coupled thermal-hydraulic and neutronic code simulating a real BWR, specifically the Swedish plant of Ringhals-1. To reach this goals we need a way to quantify the stability of the core, this is done using the DR and the NF which are detailed below.

2.1 Quantification of Instability: Decay Ratio and Natural Frequency

During normal operation of a nuclear reactor it is important to determine if it is inside the stable regime. Using the neutronics power signals obtained from APRM and LPRM we can determine the DR. If the value of the DR is between 0 and 1 , the reactor is stable because the oscillations are damping (see Figure 3). But if the DR is over 1 the reactor is unstable because the oscillations are growing (see Figure 2). The NF is the oscillation frequency of the reactor power signal. [3]

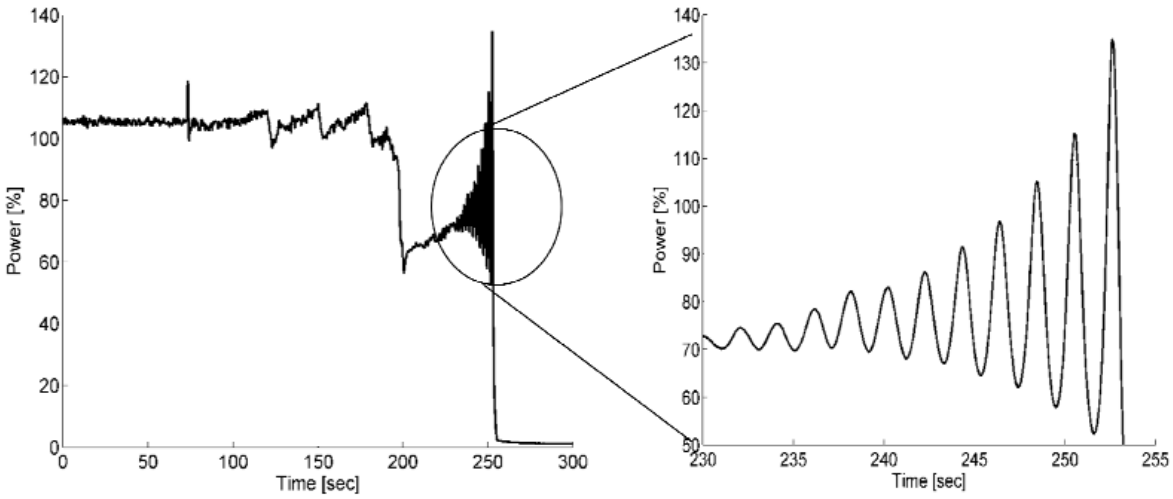

Figure 2. Oskarshamn-2 1999 event

The DR is obtained as an average of first two Bi ratios (Figure 3).

The decay ratio is defined by:

$$DR = \frac{1}{2}\left(\frac{B_2}{B_1} + \frac{B_3}{B_2}\right)$$

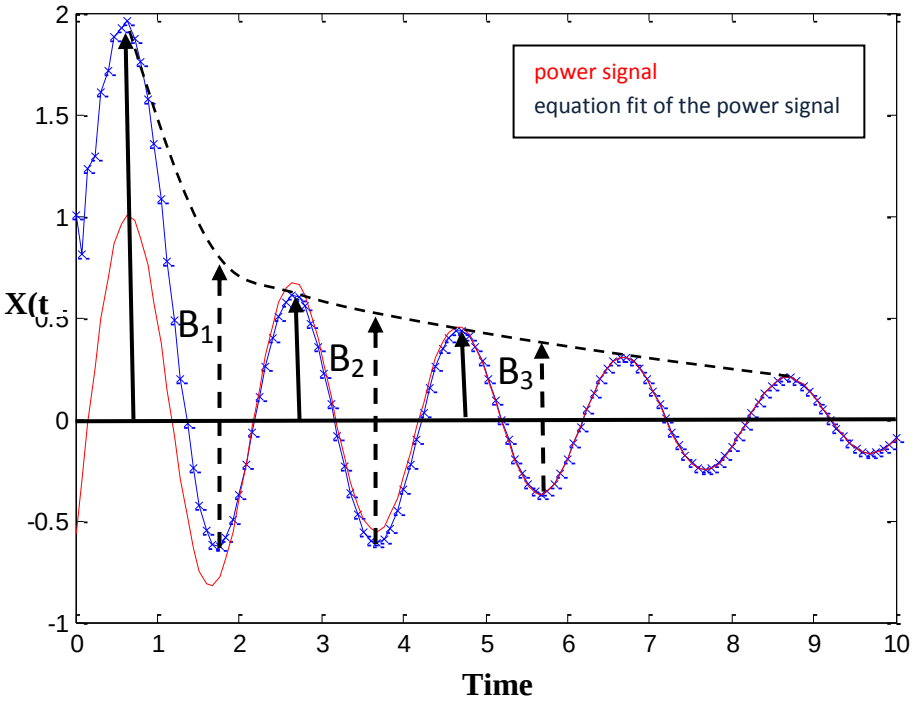

Figure 3. Definition of the Decay Ratio.

In this work we will use the software written in MATLAB called DRARMAX to calculate de DR and the NF. This package has been developed by the Purdue University and uses the output from the transient simulations to calculate the stability parameters. [5]

2.2 Ringhals-1 stability benchmark.

The Ringhals unit 1 is a Swedish BWR designed by ABB-ATOM with a nominal core power of 2270 MWth. Ringhals-1 started his commercial activity in 1976. In the frame of the OECD Ringhals-1 stability benchmark a series of stability measurements were performed for four different cycles (from the 14^{th} to the 17^{th}) with 8 to 11 points per cycle, in total 37 points with different power and flow conditions. For each point the DR and the NF were obtained. The reactor core consist of 648 fuel assemblies. Between the cycles 14^{th} to 17^{th} three different types of assemblies were loaded in the core: 8x8 assembly with 63 fuel rods, SVEA assembly with 63 or 64 fuel rods (SVEA 63 and SVEA 64). [6]

Nominal thermal power (MWt)	2270
Nominal coolant flow rate (kg/s)	7000
Nominal steam flow rate (kg/s)	1121
Number of fuel assembly	648

Table 1. Ringhals-1 NPP main properties.

In this thesis we are going to use a TRACE/PARCS model of the Ringhals-1 NPP. The model reproduces all the different cycles and points from the OECD benchmark and it has been validated. This will allow us to extract as much thermal-hydraulic and neutronic data parameters as possible from the output files of the code to associate the plant configuration with the stability response, with high confidence that the simulator data accurately represents real reactor response.

2.3 TRACE/PARCS model description.

As mentioned before, in this work, we will use the advanced computational engine known as TRACE (formerly called TRAC-M). TRACE is the latest version of advanced, best estimate reactor systems codes developed by the NRC. In this work we use the TRACE version 5.141. With this code we are able to analyze transients and steady states in light water reactors. The code is based on a non-homogeneous and non-equilibrium two-fluid model for the two phase flow conservation equations. The code solves a six field-equation model for two-phase flow:

-Conservation of mass for the liquid phase.
-Conservation of mass for the vapor phase.
-Conservation of momentum for the liquid phase.
-Conservation of momentum for the vapor phase.
-Conservation of energy for the liquid phase.
-Conservation of energy for the vapor phase.

TRACE was coupled with PARCS which is a three-dimensional neutronics core simulator code. This code was developed for the NRC by the Purdue University. This computer code solves the time-dependent two-group neutron diffusion equation in three dimensional Cartesian geometry using nodal methods to obtain the transient neutron flux distribution.

There are two classes of system codes considered in safety analysis: the frequency domain codes and the time domain codes. The frequency domain codes whose purpose is the linear stability analysis of BWR's or other boiling systems are based on linearization and Laplace transform of the governing equations. The time domain codes include analysis tools specially developed to simulate transients of NPP, they have the capability to deal with the non-linear features of BWR's and are based on the simulation techniques. TRACE is a time domain code. [3]

In this thesis we won't design any input for TRACE or PARCS but we will use previously validated input which will provide us with very good data results [3]. Since the model has been validated, the results and data extracted are realistic and similar to the ones we should find in the real installation. The TRACE/PARCS model comprises of reactor pressure vessel, fuel bundles, steam separators and dryers, steam lines, recirculation loop and a feedwater pipe.

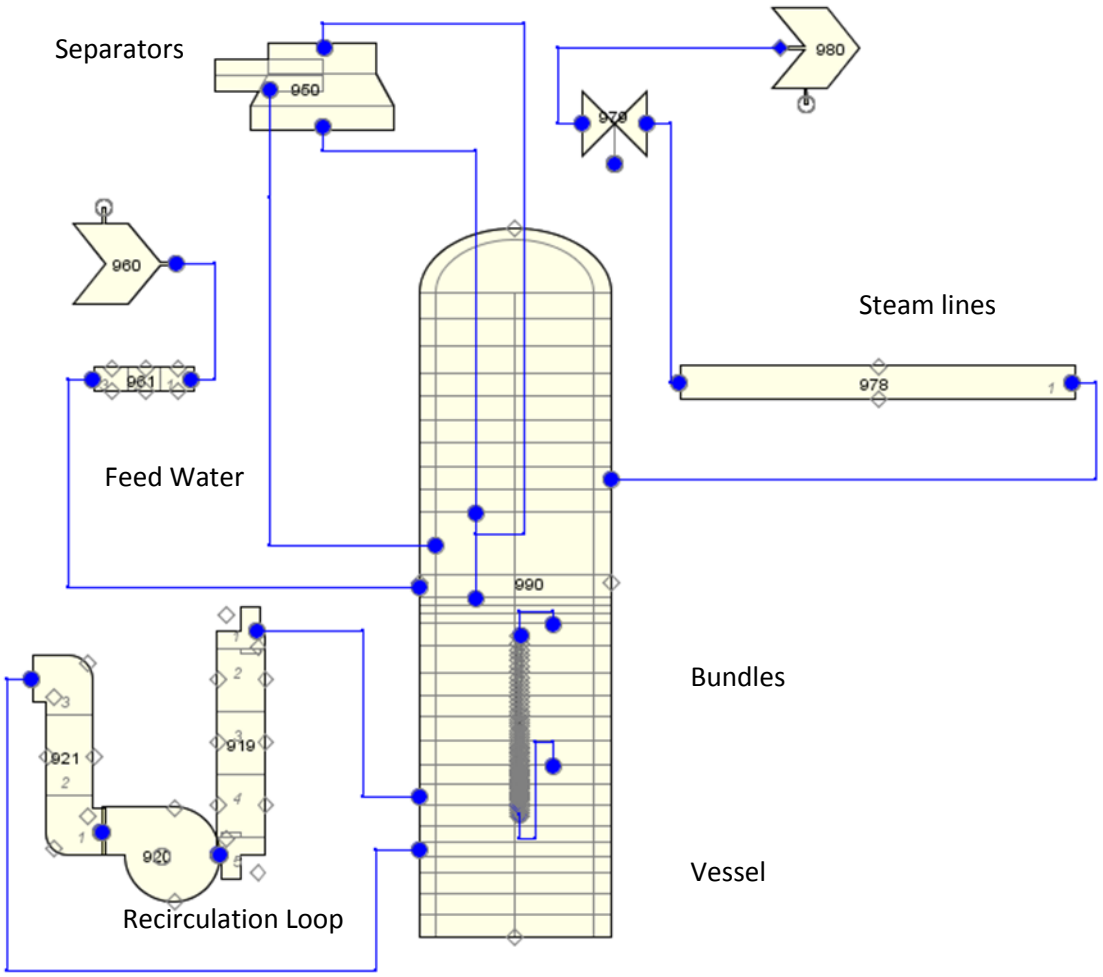

Figure 4. Nodalization scheme of Ringhals-1 NPP.

The simulation consist of, first, a steady-state with the desired flow and power conditions and second a control rod perturbation transient. Consequently, after the perturbation, the reactor will have an oscillatory behavior and, thanks to the outputs from the simulating codes, we will obtain the DR and the NF. The results are presented in the Table 2. All the obtained values from the codes matches with the experimental values, with the average DR error of 0.03.

Below we present a table (Table 2) with all the 37 experimental points simulated with the core power, core mass flow and the DR and NF obtained after the transient simulation.

Cycle/Point	Power (%)	mass flow (%)	DR measured	DR TRACE/PARCS	DR error	Fr TRACE/PARCS
C14P01	65	58,64	0,30	0,51	0,21	0,43
C14P03	65	52,37	0,60	0,65	0,05	0,42
C14P04	70	52,24	0,74	0,75	0,01	0,54
C14P05	70	55,26	0,71	0,71	0,00	0,52
C14P06	70,2	58,94	0,61	0,64	0,03	0,51
C14P08	75,1	55,49	0,80	0,79	0,01	0,51
C14P09	72,6	52,77	0,80	0,82	0,02	0,56
C14P10	77,7	58,63	0,69	0,71	0,02	0,51
C15P01	64,7	59,11	0,43	0,39	0,04	0,43
C15P02	65,2	55,44	0,46	0,39	0,07	0,41
C15P03	65,1	52,13	0,43	0,38	0,05	0,42
C15P04	70,1	59,50	0,38	0,37	0,01	0,45
C15P05	70,1	56,36	0,46	0,45	0,01	0,45
C15P06	70,3	53,93	0,61	0,60	0,01	0,47
C15P08	75,2	57,06	0,72	0,72	0,00	0,54
C15P09	71,1	51,90	0,81	0,79	0,02	0,55
C15P10	77,3	60,23	0,68	0,68	0,00	0,59
C16P01	64,3	58,74	0,60	0,59	0,01	0,48
C16P02	64,6	56,07	0,65	0,65	0,00	0,48
C16P03	64,6	52,83	0,74	0,75	0,01	0,47
C16P04	70,2	59,50	0,60	0,66	0,06	0,51
C16P05	69,9	56,04	0,70	0,74	0,04	0,49
C16P06	69,5	52,47	0,83	0,84	0,01	0,48
C16P07	74,4	58,30	0,71	0,74	0,03	0,49
C16P08	74,9	55,81	0,78	0,80	0,02	0,48
C16P09	74,6	52,54	0,90	0,90	0,00	0,47
C16P10	76	60,24	0,69	0,71	0,02	0,49
C16P11	66,1	52,19	0,81	0,79	0,03	0,50
C17P02	65,6	56,49	0,32	0,30	0,02	0,43
C17P03	65,6	52,57	0,38	0,34	0,04	0,42
C17P04	69,5	59,51	0,32	0,32	0,00	0,44
C17P05	69,9	57,36	0,35	0,35	0,00	0,44
C17P06	69,7	53,69	0,41	0,41	0,00	0,44
C17P07	74,9	59,14	0,38	0,43	0,05	0,47
C17P08	75,1	57,43	0,42	0,47	0,05	0,47
C17P09	75,4	53,41	0,52	0,60	0,08	0,47
C17P10	78,1	57,97	0,44	0,54	0,10	0,48
			DR average error		**0,03**	

Table 2. DR and NF obtained for all cycle/points.

2.4 Stability related parameters.

With the aim of study the causes of instabilities in BWR we need to collect as much relevant data as we can. Moreover, we attempt to draw the different stability maps typical of BWR plants. With the help of the literature available on this topic ([1] and [2]) we were able to collect different thermal-hydraulic and neutronic parameters affecting the stability behavior of the BWR. Some of those parameters are listed and described below.

Mass flow rate: an increase of the mass flow rate will make the reactor more stable.
Inlet subcooling: an increase of the inlet subcooling will increase the stability at high subcoolings.
Pressure: an increase in the system pressure will increase the stability.
Inlet and exit pressure drop: an increase in those pressure drops will make the reactor less stable.
Length of the channel: longer channels destabilizes the flow significantly.
Core power: the higher the power is, the more susceptible the core becomes to instability.
Axial power shape: it affects instability, a bottom peaked power shape appears to induce instability.
Void reactivity coefficient: A more negative void reactivity coefficient increases neutronics feedback directly and destabilizes the core. The void reactivity coefficient depends upon fuel design parameters (burnup, enrichment, ratio between moderator and fuel atom density).
Radial power shape: High radial power shape decreases stability.
Xe concentration: affects the stability and in particular de DR. The redistribution of the Xe concentration following a large scale power change apparently may cause a decrease of the DR.

In addition to those previous listed parameters we chose to collect other thermal-hydraulic and neutronic properties and dimensionless numbers which could have a relation with the stability behavior. At the end we were able to gather 30 different parameters, all of them are listed below and the complete database is reproduced in the Appendix.

Thermal power (%)
Thermal power (MWth)
Recirculation Pump mass Flow (kg/s)
Core mass flow rate (kg/s)
Core mass flow(%)
Density of saturated liquid phase at inlet conditions (kg/m^3)
Density of saturated vapor phase at inlet conditions(kg/m^3)
Enthalpy of saturated vapor phase at inlet conditions (kJ/kg)
Enthalpy of saturated liquid phase at inlet conditions (kJ/kg)
Inlet enthalpy(kJ/kg)
Subcooling number
Phase change number
Inlet subcooling (ºC)
Inlet saturation temperature (ºC)
Inlet temperature (K)
Inlet pressure (bar)
Inlet pressure drop (bar)
Outlet pressure drop (bar)
Core pressure drop(bar)
Radial peaking factor
axial peaking factor
Height from bottom (cm)
Plane number
Separator pressure drop (bar)
total power coefficient
Xe concentration
bypass mass flow (kg/s)
outlet void fraction
axial power offset
outlet quality

Table 3. List of parameters extracted from the simulations.

It must be noted that these parameters are all collected at the end of the steady state simulation, that is before introducing the control rod perturbation. This will reflect the state of the reactor before the oscillations are introduced and we will be able to state how the reactor is more susceptible to instabilities.

Some of these parameters represent inlet or outlet properties such as inlet enthalpy, inlet pressure, outlet pressure drop. Inlet and outlet stands for inlet of the core and outlet of the core, respectively.

Following some of the listed parameters are explained in more detail:

Subcooling number: It's a non-dimensional thermal-hydraulic parameter defined by:

$$N_{sub} = \frac{h_l - h_i}{h_g - h_l} \cdot \frac{\rho_l - \rho_g}{\rho_g}$$

where:

- h_l: saturated liquid enthalpy based on core inlet pressure.
- h_g: saturated gas enthalpy based on core inlet pressure.
- h_i: core inlet enthalpy.
- ρ_l: saturated liquid density based on core inlet pressure.
- ρ_g: saturated gas density based on core inlet pressure.

Phase change number: It's another non-dimensional thermalhydraulic parameter defined by:

$$N_{pch} = \frac{power}{\dot{m}(h_g - h_l)} \cdot \frac{\rho_l - \rho_g}{\rho_g}$$

where:

-*power*: core thermal power in Wth.
-$\dot{m}$: core mass flow rate in kg/s.
- h_l: saturated liquid enthalpy based on core inlet pressure.
- h_g: saturated gas enthalpy based on core inlet pressure.
- ρ_l: saturated liquid density based on core inlet pressure.
- ρ_g: saturated gas density based on core inlet pressure.

Inlet subcooling: It's defined as the difference of the liquid saturation temperature and the liquid bulk temperature at the core inlet.

Radial peaking factor: It's defined as the highest radial local power density divided by the average power density in the reactor core.

Axial peaking factor: It's defined as the highest axial local power density divided by the average power density in the core.

Height from bottom: This parameter gives the location of the axial peaking factor in centimeters from the bottom of the core.

Plane number: The core in the PARCS nodalization is divided in 25 axial nodes, the plane number is the number of the node where the axial peaking factor is located. The lower plane number is the number 1 and the highest correspond to the plane 25.

Total power coefficient: It's defined as

$$TPC = \frac{Keff_2 - Keff_1}{power_2 - power_1}$$

where Keff is the reactor multiplication constant and *power* is the reactor thermal power, expressed in percentage. To calculate the TPC we increase the reactor power by 1% and we extract the multiplication constant before and after the power increase. TPC combines the effect of the Doppler coefficient, the temperature coefficient, moderator coefficient and the void coefficient.

Outlet void fraction: It describes the amount of the vapor phase in the two-phase flow. The outlet void fraction describes the volumetric content of the vapor phase in the mixture.

Axial power offset: It's a parameter that represents the axial power shape of the core, it's defined as:

$$APO = \frac{\sum top\ half\ axial\ peaking\ factors}{\sum bottom\ half\ axial\ peaking\ factors}$$

If the APO is bigger than 1, the axial power shape of the core is top peaked. If the APO is smaller than 1 the core is bottom peaked.

Outlet quality: It also describes the amount of the vapor phase in a two-phase flow. But, in this case, the outlet quality is a measure of the mass flow of vapor in the mixture:

$$Outlet\ quality = \frac{\dot{m}_v}{\dot{m}_v + \dot{m}_l}$$

3. RESULTS

3.1 Stability maps.

Two typical stability maps are used to represent the unstable operating areas of the reactor. Those maps are the power-flow map and the dimensionless heat flux (Npch) versus the inlet subcooling (Nsub) map. These maps give to the plant operators some basic information about the expected oscillatory behavior of the plant. However, these maps are not totally accurate and we can expect to find instability issues even though the plant is supposed to operate in a stable zone. For the aim of this work, after collecting all the data of the 37 measured Ringhals-1 points, we draw the stability maps in way to find their deficiencies.

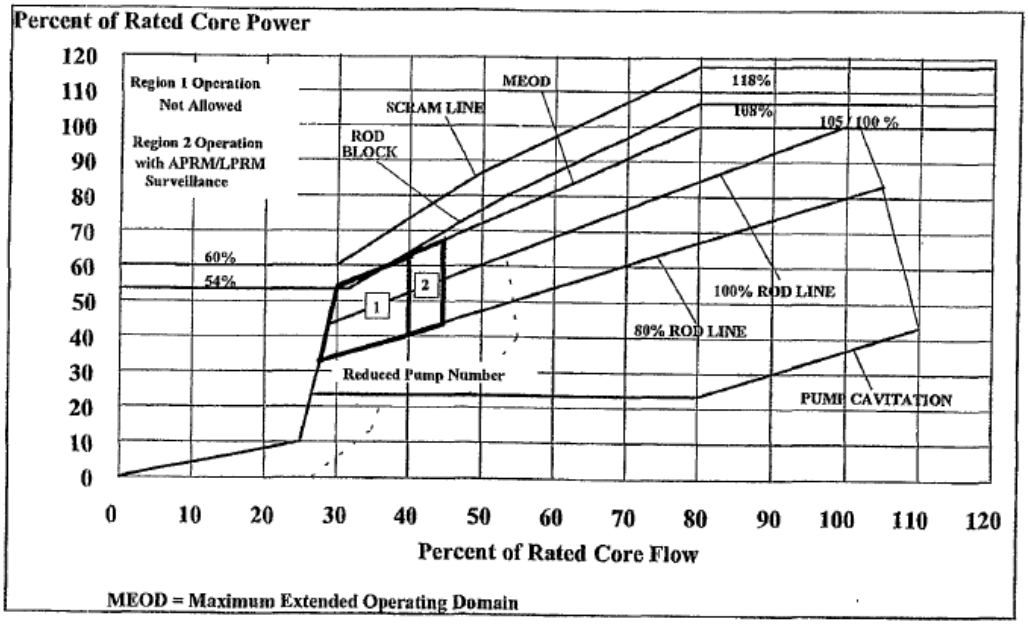

Figure 5. Typical BWR operating Power-Flow map [1]

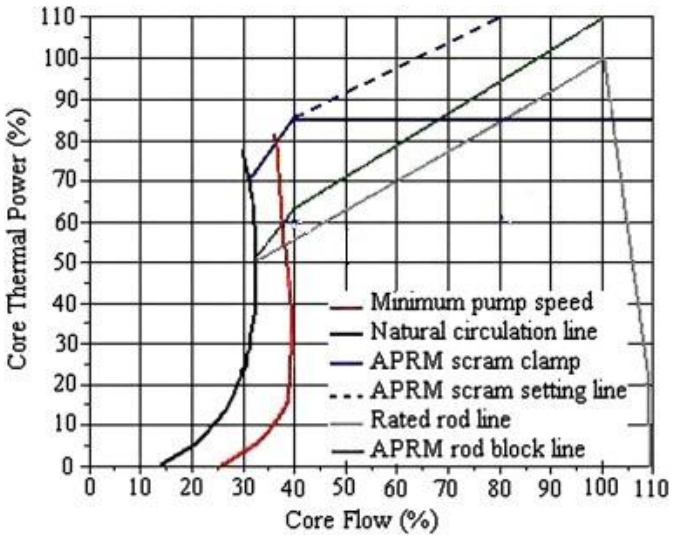

Figure 6. Power-Flow map from the Peach-Bottom 2 Npp [7]

Above we can see two figures showing two different Power-Flow stability maps. We know that the instability should be in the zone with relatively low core flow and high core power while the stable zone is located where the core flow is relatively high and the power is low.

Using the data extracted from the simulations (core mass flow, core power and DR) we are able to draw the stability map of Ringhals-1. Moreover, thanks to the stability benchmark [6] previous work we can trace the operating boundaries (represented as a red line in the graph) of the plant. The result is showed in the next figure (Figure 7). We can see how stability boundary is not perfect in the sense that we can find unstable points in zones where they are not suppose to be. That proves the lack of accuracy of this kind of stability maps. This is due to the fact that those graphs represent only two parameters, while we know that instabilities are affected by other triggers. Next to every one of the 37 measured Ringhals-1 points we show the DR and the name of the point. That allow us to locate anomalies in the graph. For example, we can check on the graph how the point C14P03 with a DR of 0.65 (high value) is very close to the points C15P03 and C17P03 with much lower DR of 0.38 and 0.34 respectively. That shows how, for very similar power and flow conditions, the behavior of the oscillations could be very different. Another example from the same graph are the point C16P01 with a DR of 0.59 and the point C15P05 with a lower DR of 0.39. Despite that these points are located next to each other in the graph (low power- high mass flow) they have very different DR.

The second kind of stability map has also been plotted (Figure 8) using the data extracted from the simulations. In this map the points with similar DR are supposed to be located in the same bands (between the blue lines). Those bands group the points with the same DR and the bands on the left side are those of the smaller DR's while as we move to the right the DR's grow. The same problem appears in this stability map and we can find points with DR in positions where they are not consistent. Some examples of the anomalies are the points C16P10 with a DR of 0.71, the point C16P07 with a DR of 0.74 and the point C17P07 which has a much lower DR of 0.43. These points have very similar Npch and Nsub but a very different DR. The points in conflict are highlighted in the plots.

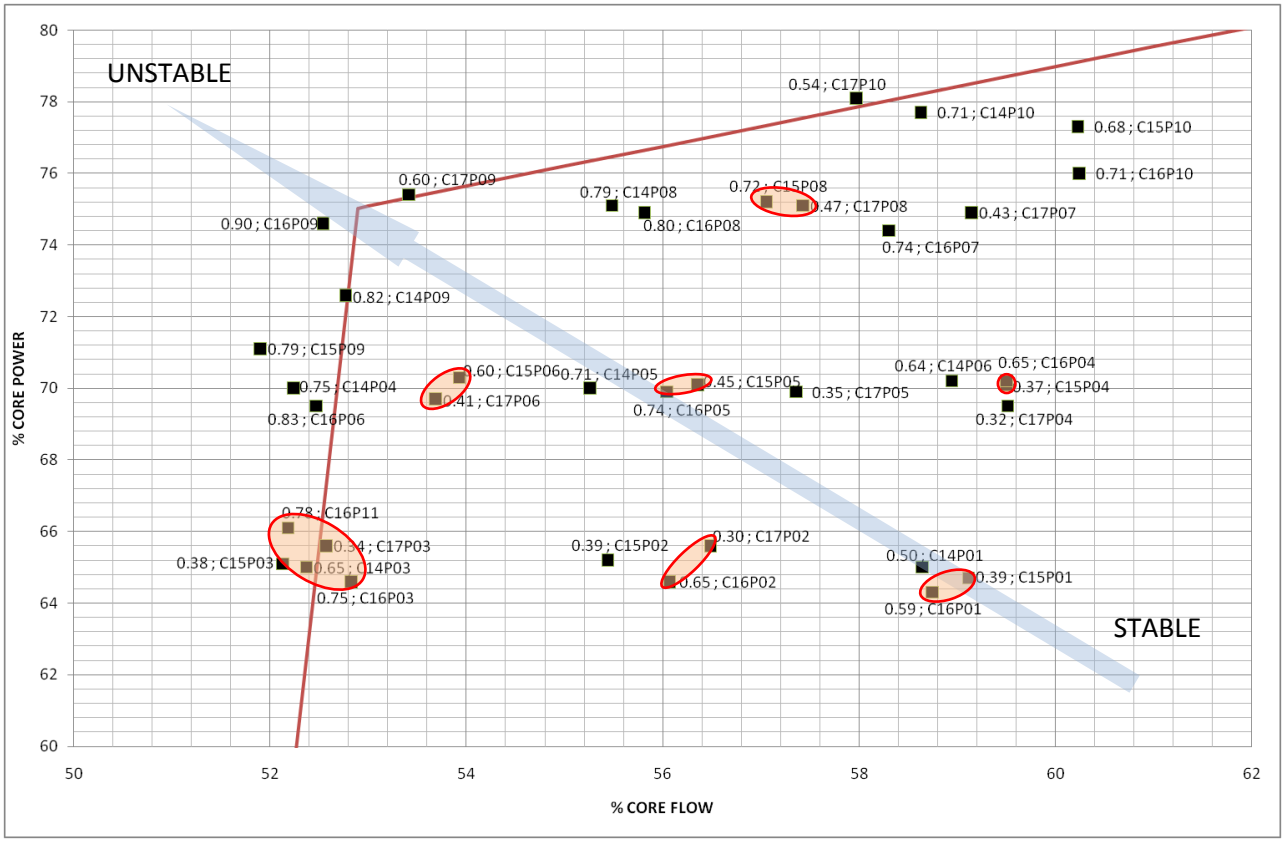

Figure 7. Ringhals-1 Power-Flow map with the 37 data points.

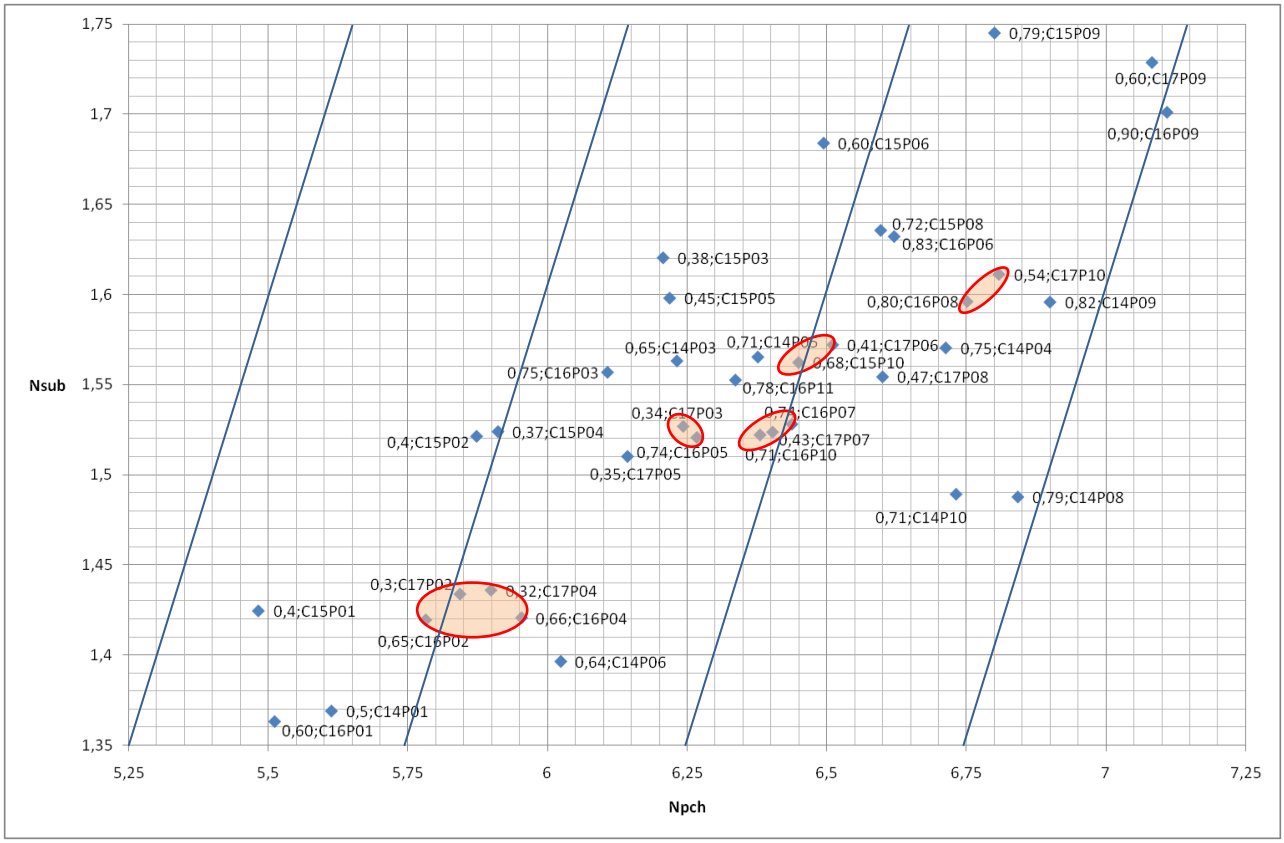

Figure 8. Ringhals-1 Npch-Nsub stability map.

3.2 Multiple linear regression analysis.

As we can see from the stability maps obtained after the Ringhals-1 data it's obvious that, in aim to predict the DR of the oscillations appearing in the core, more parameters should be studied and new stability maps proposed. For that purpose, in this work, we realize this goal through a multiple linear regression analysis.

Multiple linear regression is a method to model the relationship between two or more explanatory variables and a response variable by fitting a linear equation to observed data. In our case the variable response is the DR that represents the stability, while the explanatory variables are all 30 variables extracted from TRACE and PARCS shown in Table 3. Every value of the independent variable x is associated with a value of the response variable DR. Having n explanatory variables x_1, x_2, …, x_n and an infinite set of data (explanatory variables and response data), the regression equation should be: $Y = B_0 + B_1 x_1 + B_2 x_2 + \cdots + B_n x_n$, but since we don't have all the values and that the values we have may not be perfectly accurate, the estimated regression will be:

$$DR = b_0 + b_1 x_1 + b_2 x_2 + \cdots + b_n x_n + E$$

In this equation, b_i is the fitted value of B_i and E is the residual term which represents the deviation between the values and the fitted values from the equation (DATA=FIT+RESIDUAL). The way to find the best regression equation is to look for the one which minimizes the sum of the squares of the deviations (residual). To find a suitable regression equation the different variables must be independent.

In this work we will use a statistical software known as MINITAB which will help us to find different regression equations with a different number of variables.

First, we achieve an exploratory study over the different parameters to see if we can find one which is very related with the DR or to see if some transformation of the response variable or any of the explicative variables could be interesting. No transformation of any of the variables seems to improve the linear regression between them and the DR and no transformation of the response variable DR seems helpful either.

Scatter plots between the explicative variables show that some of them are dependent with other explicative variables, those variables are: the enthalpies, the inlet temperatures, the inlet pressure and the inlet densities. These variables cannot appear at the same regression model together or any combination of them.

In a first exploration of the data any variable, alone, seems to be very related with the DR as we can see in the plots below. Despite of that, it's possible to find a combination of various variables that could lead to a better prediction of the response variable.

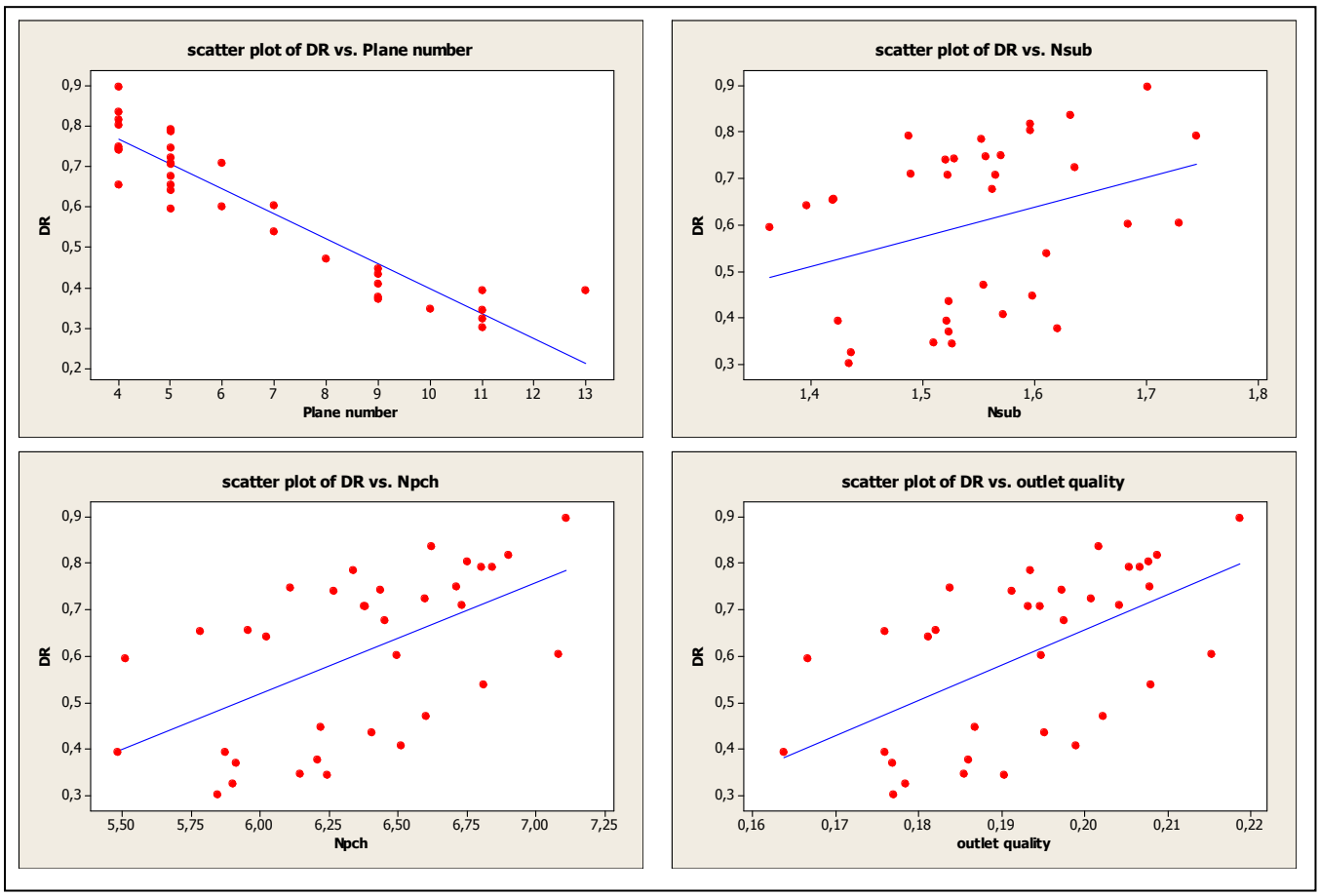

Figure 9. Plots of some explicative variables against the response: DR.

Once we know which variables are independent we can proceed to search for the best regression equations. For this we will use a method called *Best Subsets*. This tool inside the MINITAB software looks for the best fitting variables combinig them starting with the best linear regression and proceeding with increasing the number of explicative variables. After we find the best regression we will try to improve them finding the points introducing the biggest deviation (difference between the real DR value and the one predicted by the regression equation).

With the help of another tool in the same statistic software called *stepwise*, we can reduce the number of explicative variables to introduce in the *Best Subsets*. The *stepwise* can handle all the 30 variables, even if some of them are dependent. The *stepwise* is introducing and removing variables if they are improving the model or, when a new variable is introduced and it deteriorates the model, it's removed. The process ends when no new variables can be introduced.

After the results from the *stepwise* we decide to do a *Best Subsets* with the next set of variables which seems to be the ones which can predict the DR with a high accuracy (highest R-square value).

-Mass Flow (%)
-Subcooling Number (Nsub)
-Phase Change Number (Npch)
-Radial Peaking Factor
-Axial Peaking Factor
-Plane Number
-Axial Power Offset
-Total Power Coefficient (TPC)
-Core Power (%)
-Separator Pressure Drop (bar)

The output from MATLAB is showed below:

Best subsets:

The predicted variable is DR

Vars	R-squa.	R-squa. (adjusted)	Cp of Mallows	S	mass flow %	Nsub	Npch	radial	axial	plane	power	TPC	Power (%)	ΔP-separator (bar)
1	51,5	50,1	22,7	0,12268					X					
1	50,5	49,0	23,9	0,12402				X						
2	61,1	58,8	13,7	0,11155				X	X					
2	57,1	54,5	18,3	0,11714			X		X					
3	64,9	61,7	11,3	0,10756			X		X	X				
3	63,6	60,3	12,8	0,10945		X			X	X				
4	68,5	64,6	9,2	0,10341		X	X		X	X				
4	67,6	63,5	10,2	0,10495		X	X		X		X			
5	72,0	67,4	7,2	0,099121		X	X		X	X	X			
5	71,6	67,1	7,6	0,099690		X	X		X		X			X
6	74,7	69,6	6,0	0,095717	X	X	X		X	X	X			
6	74,6	69,5	6,1	0,095896	X	X	X		X		X			X
7	76,7	71,0	5,8	0,093496	X	X	X		X	X	X			X
7	76,6	70,9	5,9	0,093700	X		X	X	X	X	X	X		
8	77,1	70,6	7,3	0,094246	X		X	X	X	X	X	X	X	X
8	76,8	70,2	7,6	0,094830	X	X	X	X	X		X	X		X
9	77,3	69,8	9,0	0,095499	X	X	X	X	X	X	X	X	X	X
9	77,1	69,5	9,3	0,095969	X		X	X	X	X	X	X	X	X
10	77,4	68,6	11,0	0,097287	X	X	X	X	X	X	X	X	X	X

Figure 10: Best Subsets output with 37 data points

We can observe from the previous output how we aren't able to predict with more than a 70% of accuracy the DR with the chosen variables. This can be due to the fact that the variables aren't good enough or maybe some of the points can't fit properly in the model, introducing a large error. To check this, we run the regressions with 2 to 4 variables from the *Best Subsets* output. We observe how the first data point, corresponding with the simulated point C14P01 is always introducing a big error in the model. In the next figure (Figure 11) we can see how the standardized residue of the point C14P01 is almost 3, while the standardized residues must be between -2 and 2.

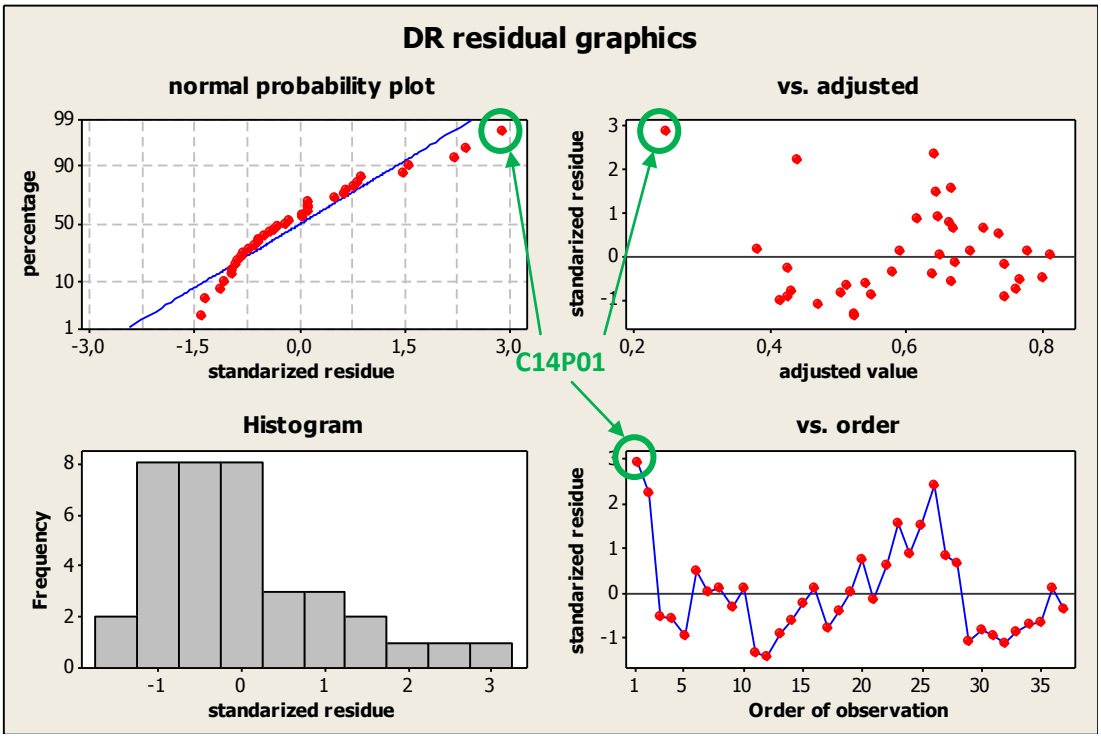

Figure 11: DR residual graphics with 37 data points

So, after this observation, we decide to remove the point C14P01 from the data set and do the *Best Subsets* again with the same variables. The results are improving but we aren't able to reach more than a 75.8 % of accuracy with four explicative variables. Taking a look on the residual graphics we notice that, without the point C14P01, the point C14P03 is now introducing a big deviation. So we decide to remove it also and do the next set of regressions with 35 of the initial 37 points.

Now, with only 35 points, the regressions are significantly improved and with only 2 variables we can obtain a 90,9% of accuracy. The output from the *Best Subsets* is shown in Figure 12 where we can see that with 4 variables the accuracy of the prediction is already 93,4% .

The predicted variable is DR

Vars	R-squa.	R-squa. (adjusted)	Cp of Mallows	S	mass flow %	Nsub	Nspch	radial peak	axial peak	Plane number	axial power offset	TPC	Power (%)	ΔP-separator (bar)
1	85,9	85,5	37,6	0,067724						X				
1	52,3	50,8	201,7	0,12469							X			
2	91,4	90,9	12,8	0,053653				X		X				
2	88,4	87,7	27,3	0,062280	X					X				
3	93,3	92,7	5,5	0,048045	X			X		X				
3	92,5	91,8	9,3	0,050826		X		X		X				
4	94,2	93,4	3,3	0,045609	X			X		X		X		
4	93,6	92,7	6,4	0,048044			X	X		X			X	
5	94,9	94,1	1,7	0,043321			X	X		X		X	X	
5	94,9	94,0	1,8	0,043457	X			X		X		X	X	
6	95,0	93,9	3,4	0,043791			X	X	X	X		X	X	
6	95,0	93,9	3,4	0,043863			X	X		X	X	X	X	
7	95,1	93,8	5,0	0,044297			X	X	X	X		X	X	X
7	95,1	93,8	5,1	0,044338			X	X		X	X	X	X	X
8	95,1	93,6	7,0	0,045131			X	X	X	X	X	X	X	X
8	95,1	93,6	7,0	0,045132		X	X	X	X	X		X	X	X
9	95,1	93,3	9,0	0,046014		X	X	X	X	X	X	X	X	X
9	95,1	93,3	9,0	0,046018	X	X	X	X	X	X		X	X	X
10	95,1	93,0	11,0	0,046957	X	X	X	X	X	X	X	X	X	X

Figure 12: Best Subsets output with 35 data points.

In the next table (Table 4) are collected the final results of the simulations with 35 data points. These regression equations are the best ones found during this work. Additional modifications in the regression variables did not result in improvements.

Thanks to the obtained regression equations, we will be able to draw new stabilty plots that may be of interest.

Data	Number of variables	Variables	Observations	R^2 adj
35 points	2	Radial Peak Plane Number	35	90,90%
	2	Mass Flow % Plane Number	35	87,70%
	3	Mass Flow % Radial Peak Plane Number	35	92,70%
	3	Nsub Radial Peak Plane Number	35	91,80%
	4	Mass Flow % Radial Peak Plane Number TPC	35	93,40%
	4	Npch Radial Peak Plane Number Power %	35	92,70%

Table 4. Summary table of the multiple linear regression analysis with 35 data points.

The variables that, in the case of the data set from Ringhals-1 stability benchmark, are more related with the stability behavior are the radial peaking factor, the plane number where the maximum axial peaking factor is located and the core mass flow rate.

3.3 Graphical representation.

In this section we will achieve the final objective of this work: to develop new graphical representations of the instability behavior of the BWR. As said in the previous chapter, for that purpose, we will use the regression equations found that can explain and predict the DR obtained during the Ringhals-1 experiments.

The first equation used is the one that have only two explicative variables and a R-square accuracy of 90,9 %. The equation [1] is:

$$DR = 4.373 - 0.071498 * PlaneNumber - 2.02 * RadialPeakingFactor \quad [1]$$

The variables are the plane number where the maximum axial peaking factor is located and the radial peaking factor. These two variables are purely neutronics. The previous equation is showed in Figure 13 . To help to visualize the trend in this plot we also draw the equation plane in Figure 14.

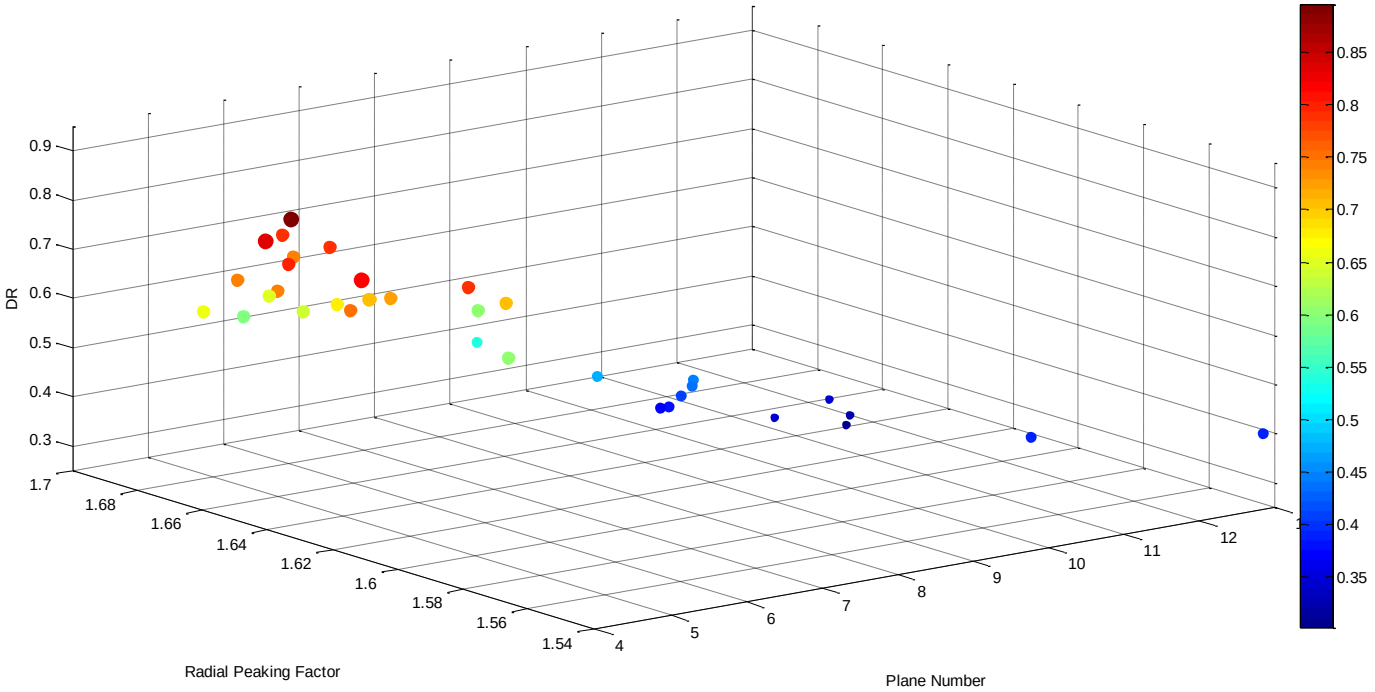

Figure 13. DR as a function of the Plane Number and the Radial Peaking Factor.

In the previous plot the colors are related with the DR, so the blue tones represents low DR (stable situations) and the red colors are for high DR (unstable configurations). Due to the fact that we are showing a three-dimensional plot it is complicated to apreciate the trend and the exact location of the points.

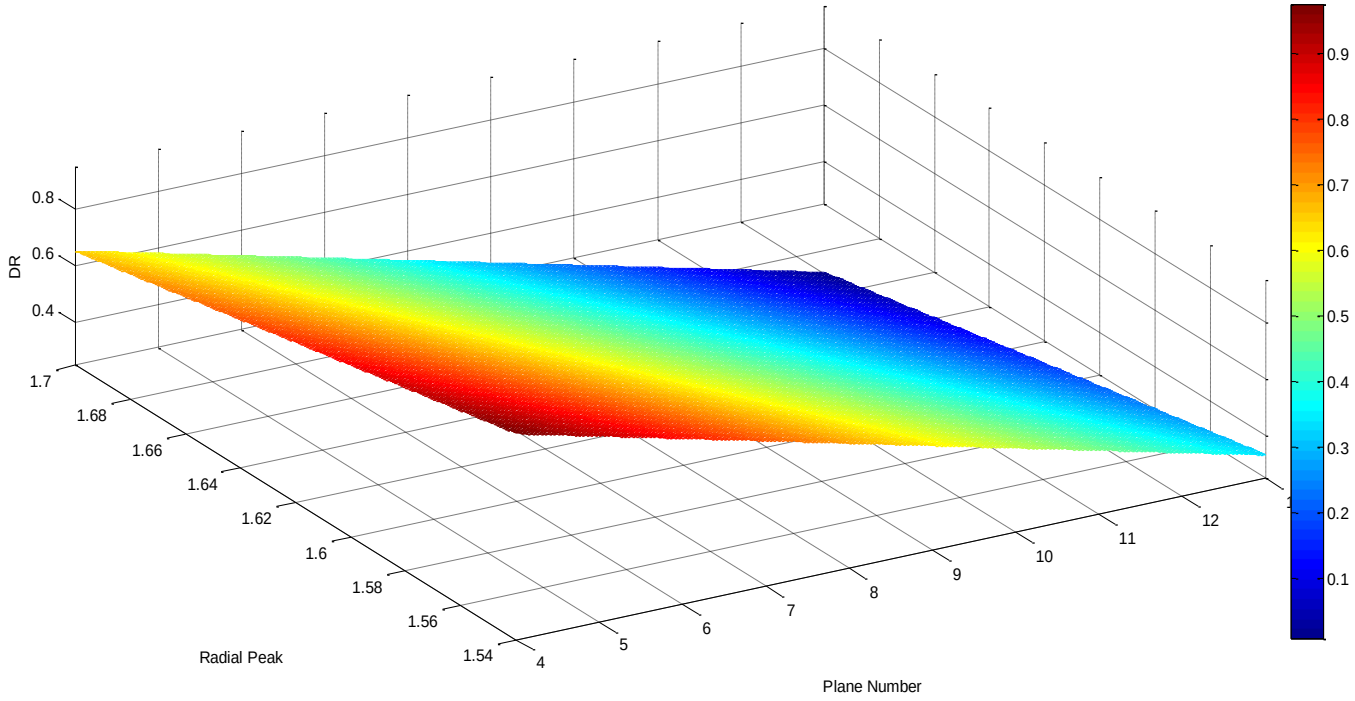

Figure 14. Plane of equation [1].

Form the previous figure (Figure 14) we can observe the trend of the DR as a function of the regression variables more clearly. For higher positions of the maximum axial peaking factor combined with a high radial peaking factor the DR is minimum while if we reduce both variables the DR increases. We have to consider that this trend is only valid between the limit values of our parameters.

Following, we repeat the same process of plotting with the second two-variables equation with R-square accuracy of 87,7%. In this case the regression variables are the Plane Number where the maximum axial peaking factor is located and the core mass flow. So, in this second equation are represented both thermalhydraulic and neutronic factors. The regression equation [2] is:

$$DR = 1.58 - 0.0599 * PlaneNumber - 0.0103 * MassFlow \text{ [2]}$$

We plot, as before, the real data points and the regression plane in the following two figures (Figures 15 and 16).

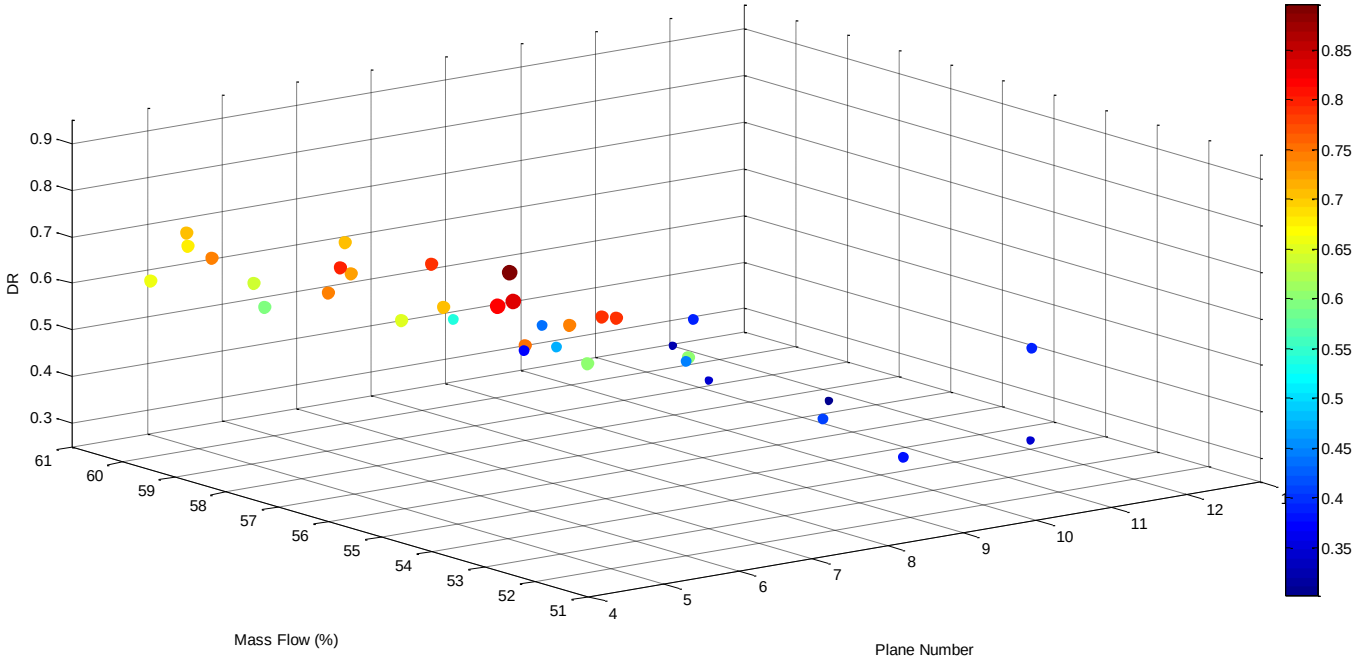

Figure 15. DR as a function of the Plane Number and the Mass Flow.

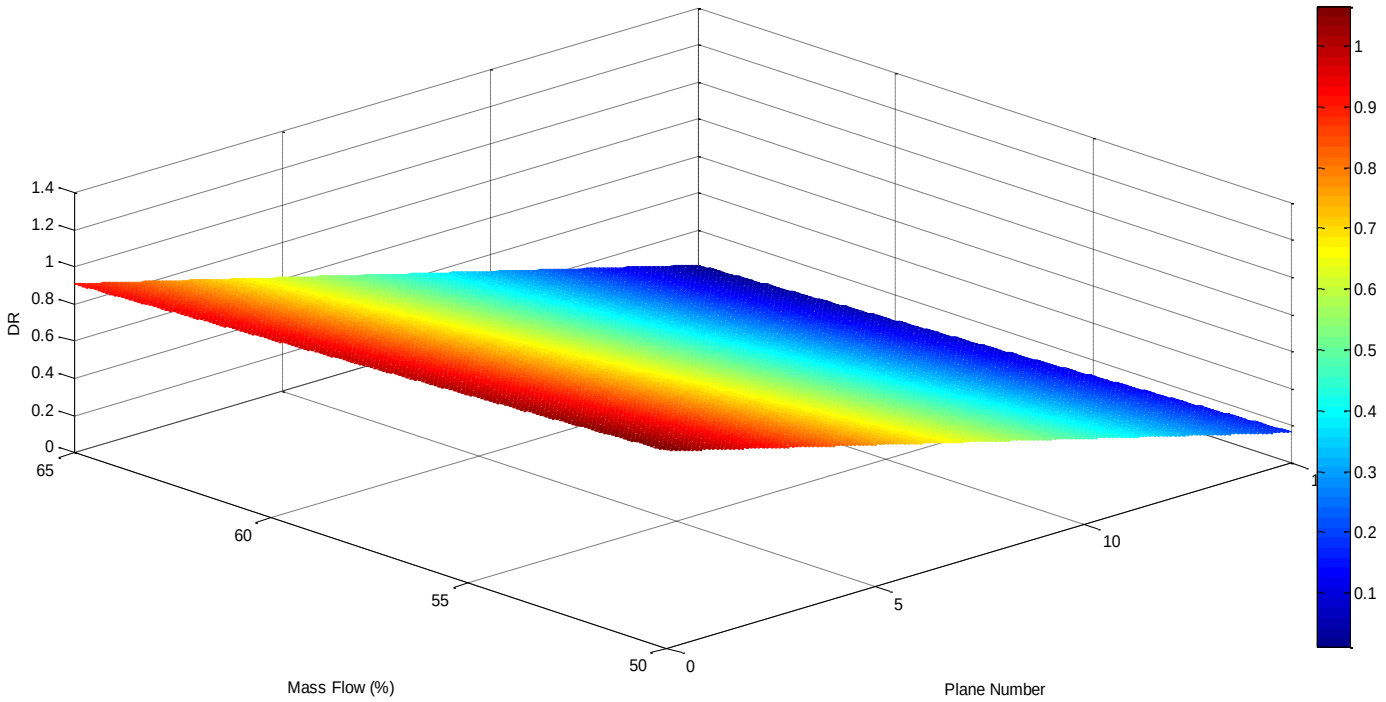

Figure 16. Plane of equation [2].

We observe that with lower core mass flows and a bottom peaked axial power shape the core tend to be more unstable.

Following we are going to plot and represent the regression equations with three explanatory variables. The first one predict the DR with an accuracy of 92,7% from the radial peaking factor, the core mass flow and the plane number where the maximum axial peaking factor is located. The regression equation [3] is:

$$DR = 4.68 - 0.0696 * PlaneNumber - 0.00895 * MassFlow - 1.91 * RadialPeak \quad [3]$$

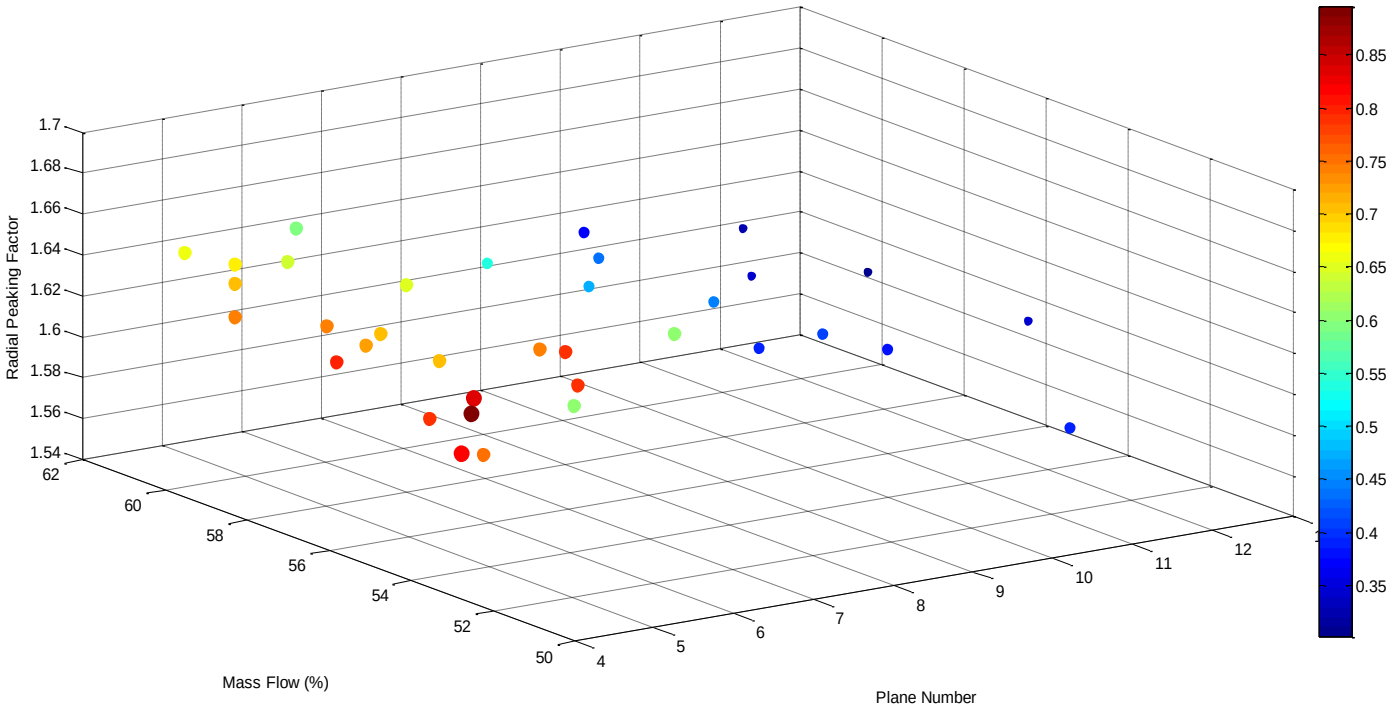

Figure 17. DR as a function of the Plane Number, the Nsub and the core Mass Flow.

From this plot we can see how, as before, bottom peaked axial core power shapes and low core mass flow rates make the core more unstable. The third parameter, the radial peaking factor, seems to not have a strong relation with the variation of the DR, but if we compare the regression from equation [2] the addition of this parameter increase the accuracy of the prediction five percent.

The second regression with three explanatory variables predict the DR with a R-square accuracy of 91.8%. The variables are the subcooling number, the radial peaking factor and the plane number where the maximum axial peaking factor is located. The regression equation [4] is:

$$DR = 3.81 - 0.0693 * PlaneNumber + 0.211 * Nsub - 1.88 * RadialPeak \quad [4]$$

This equation has been plotted in the next figure (Figure 18).

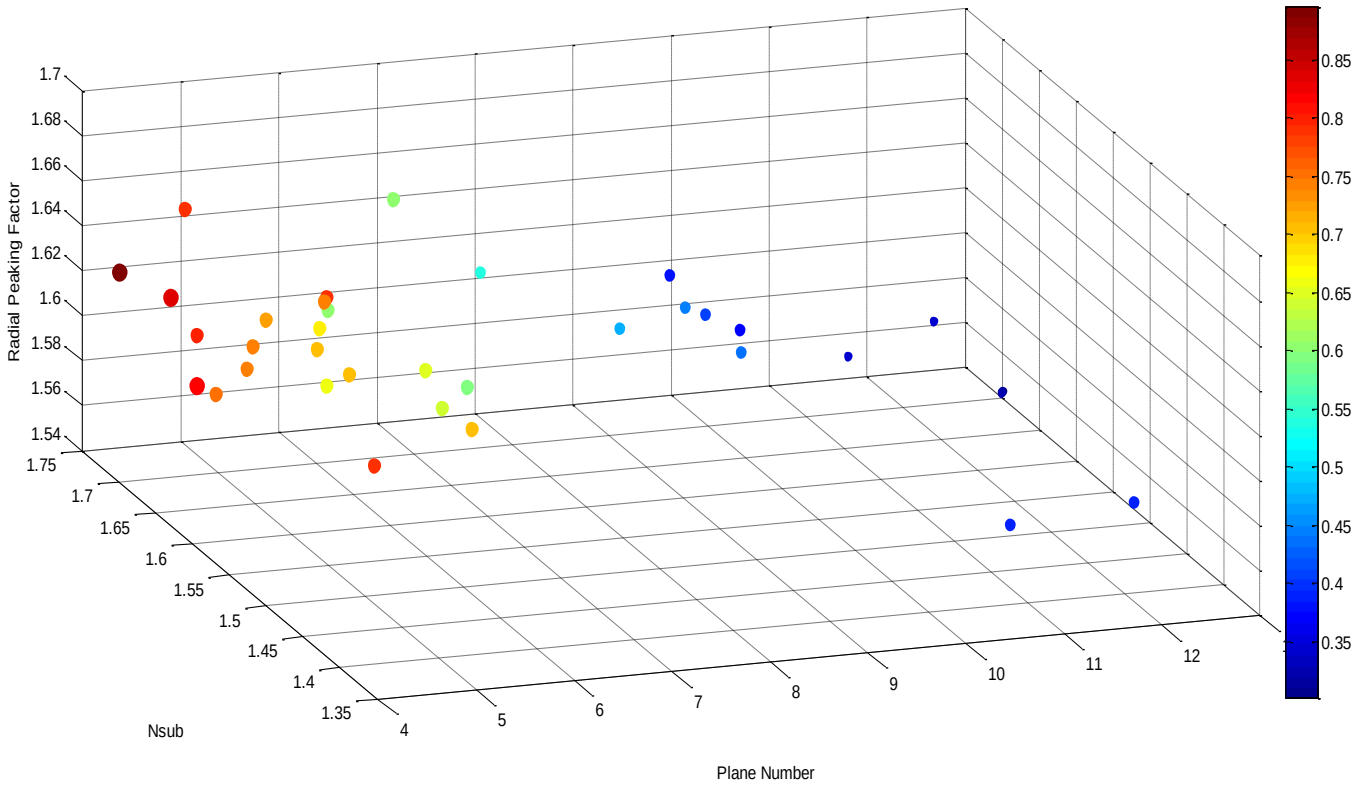

Figure 18. Plot of the regression equation [4].

This last equation includes for the first time, compared with the previous ones, the subcooling number. This parameter is not highly correlated with the DR, but we found that the DR is higher when the subcooling number increases. We observe that this statement is opposed to the one found in the literature ([1] and [2]). In the literature it's stated that an increase in the inlet subcooling will increase the stability at high subcoolings. This difference can be explained if we take a look to the shape of the Nsub-Npch stability map (Figure 19). In this figure we can see how for lower Npch and lower Nsub, an increase of the Nsub makes the system more unstable (from point 1 to point 2) while for lower Npch and higher Nsub, an increase of the Nsub makes the system more stable (from point 2 to point 3). If we observe the values of the Nsub and the Npch extracted from the 37 measured Ringhals-1 points (see Appendix) we can observe how the Nsub is between 1,40 and 1,75 and the Npch is between 5,02 and 6,33. Which are values around the point 1 in Figure 19.

The previous plotted regression (equation [4]) has the same variables as the first regression (equation [1]) plus the subcooling number. The addition of this variable only increase the prediction of the equation in less than one percent.

The data extracted from the simulations prove to be helpful and gives us the way to plot new stability maps. These plots and regressions can be improved using a bigger data population which, as we did here, can be extracted from validated plant models.

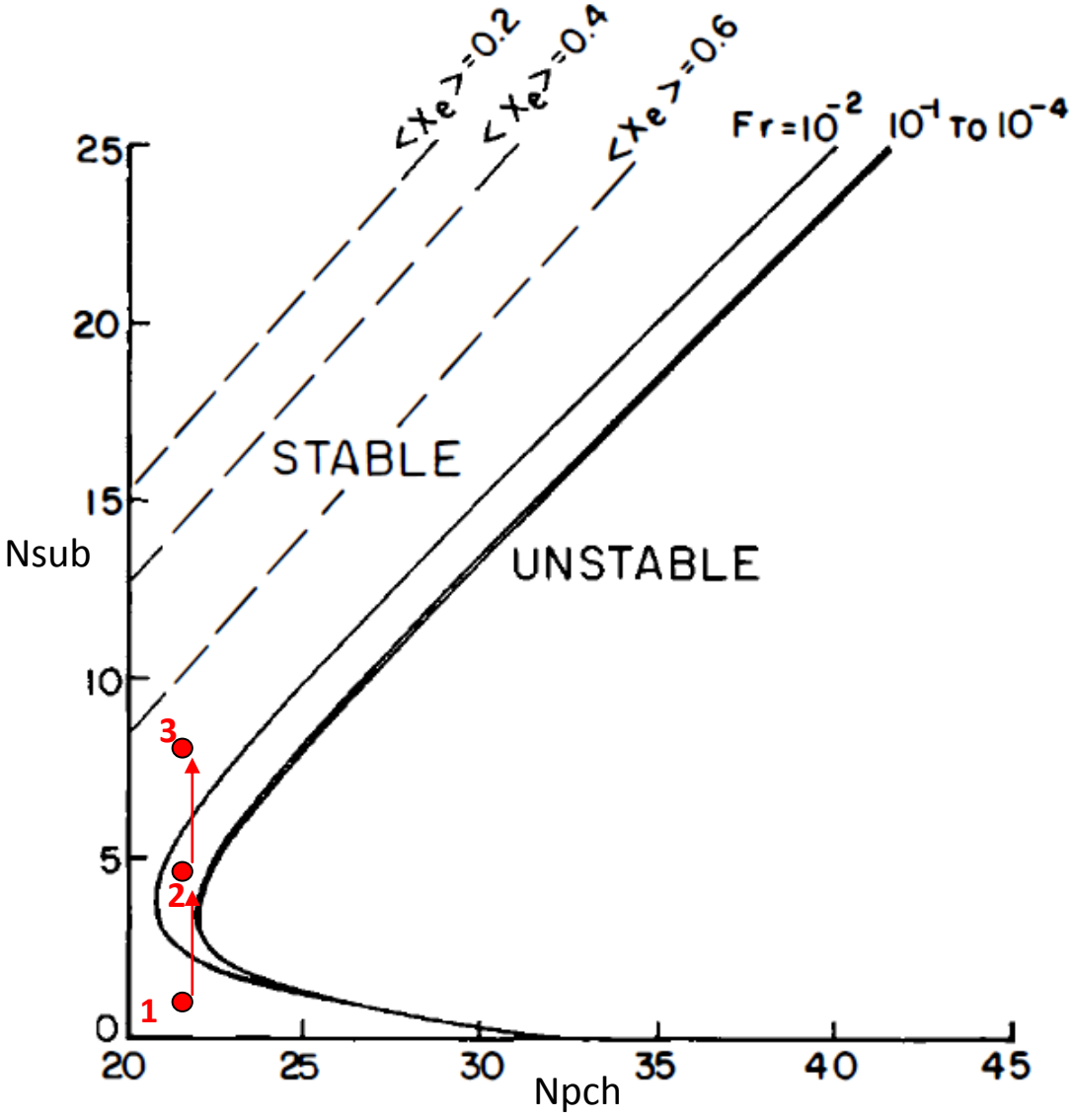

Figure 19: Typical BWR Nsub-Npch stability-map. [8]

4. CONCLUSIONS

BWR instability events have long been a concern in the nuclear industry. The study and understating of this phenomena needs knowledge in various fields of nuclear sciences as neutronics, thermal-hydraulics but also mathematics and computational sciences, which makes this a challenging multidisciplinary research area. In this work we have experienced the difficulties of treating with this subject. Thanks to the neutronics-thermal-hydraulic simulation tools and data analysis software we have been able to find the most stability related parameters from the Ringhals-1 benchmark experiments and we have been able to plot new stability graphs.

We have found different regressions with an R-square accuracy higher than 90% using the plant data from the Ringhals-1 benchmark. It has to be noticed that this equations are valid only between the boundary values of core flow and core power simulated during the benchmark. We compare the relation between those parameters and the DR from the literature with the relation found thanks to the multiple linear regression models. Both relations follows the same trends. The results are consistent.

After this study we can highlight the importance of the following parameters: the power shape, the core mass flow, the core power, the neutronics feedback (TPC) and the inlet subcooling as the important actors in the stability response. In the models found in this thesis the axial power shape and the radial peaking factor were the main parameters capable to predict the DR of the oscillations after the control rod perturbation. Neutronic influenced instabilities have to been taking into account when new fuel elements and core fuel configurations are designed.

To be able to improve the quality of the predictions made in this thesis, a bigger data population is needed. This could be achieved with more transient simulations using, as we did, validated plant models which have proved to be a reliable tool.

REFERENCES

[1] D'Auria F. , Ambrossini W., Anegawa T., 1997: State of The Art Report on Boiling Water Reactor Stability (SOAR ON BWRS). Committee on the Safety of Nuclear Installations. OECD Nuclear Energy Agency (NEA).

[2] Rui Hu, Mujid S. Kazimi, 2010: Stability Analysis of the Boiling Water Reactor: Methods and Advanced Designs. Center for Advanced Nuclear Energy Systems (CANES). Massachusetts Institute of Technology, Cambridge USA.

[3] Gajev I., 2010: Sensitivity and Uncertainty Analysis of BWR Stability, Licentiate Thesis in Energy Technology, KTH, Stockholm SWEDEN.

[4] March-Leuba J., Rey J.M., 1993: Coupled Thermalhydraulic-neutronic Instabilities in Boiling Water Nuclear Reactors: a Review of the State of the Art. Nuclear Engineering and Design, Volume 145, Issues 1-2, Pages 97-111.

[5] Yunlin Xu, 2005: DRARMAX MANUAL, Purdue University, Indiana, USA.

[6] Lefvert T., 1996: Ringhals-1 Stability Benchmark Final Report, Vattenfall AB Electric Generation SWEDEN , NEA Nuclear Science committee.

[7] Humberto V. Soares, Antonella L. Costa, 2010: Valuation of BWR Stability Operating in Natural Circulation Conditions, Journal of Progress in Nuclear Energy edited by: T.D. Beynon and D.J. Dudziak.

[8] Dr. R. T. Lahey, Jr. , Dr F. J. Moody, 1977: The Thermal-Hydraulics of a Boiling Water Nuclear Reactor, American Nuclear Society, La Grange Park, Illinois, USA.

APPENDIX

In the following pages we can find the totality of the data base used in this work. The values are extracted from the outputs of TRACE and PARCS at the end of the steady-state simulation.

Cycle/Point	Power (%)	thermal power MWth	Recirculation Pump mass Flow (kg/s)	Core mass flow rate (kg/s)	DR	Fr
C14P01	65,00	1475,50	4105	3724,40	0,51	0,43
C14P03	65,00	1475,50	3666	3356,66	0,65	0,42
C14P04	70,00	1589,00	3657	3350,61	0,75	0,54
C14P05	70,00	1589,00	3868	3525,95	0,71	0,52
C14P06	70,20	1593,54	4126	3741,18	0,64	0,51
C14P08	75,10	1704,77	3884	3535,49	0,79	0,51
C14P09	72,60	1648,02	3694	3380,71	0,82	0,56
C14P10	77,70	1763,79	4104	3716,09	0,71	0,51
C15P01	64,70	1468,69	4138	3748,76	0,39	0,43
C15P02	65,20	1480,04	3881	3530,37	0,39	0,41
C15P03	65,10	1477,77	3649	3335,98	0,38	0,42
C15P04	70,10	1591,27	4165	3767,83	0,37	0,45
C15P05	70,10	1591,27	3945	3582,39	0,45	0,45
C15P06	70,30	1595,81	3775	3441,21	0,60	0,47
C15P08	75,20	1707,04	3994	3622,25	0,72	0,54
C15P09	71,10	1613,97	3633	3324,70	0,79	0,55
C15P10	77,30	1754,71	4216	3806,41	0,68	0,59
C16P01	64,30	1459,61	4112	3735,79	0,59	0,48
C16P02	64,60	1466,42	3925	3577,98	0,65	0,48
C16P03	64,60	1466,42	3698	3388,69	0,75	0,47
C16P04	70,20	1593,54	4165	3774,70	0,66	0,51
C16P05	69,90	1586,73	3923	3571,22	0,74	0,49
C16P06	69,50	1577,65	3673	3362,89	0,84	0,48
C16P07	74,40	1688,88	4081	3699,08	0,74	0,49
C16P08	74,90	1700,23	3907	3552,09	0,80	0,48
C16P09	74,60	1693,42	3678	3361,17	0,90	0,47
C16P10	76,00	1725,20	4217	3812,15	0,71	0,49
C16P11	66,10	1500,47	3653	3347,17	0,79	0,50
C17P02	65,60	1489,12	3954	3601,08	0,30	0,43
C17P03	65,60	1489,12	3680	3372,25	0,34	0,42
C17P04	69,50	1577,65	4166	3776,62	0,32	0,44
C17P05	69,90	1586,73	4015	3649,02	0,35	0,44
C17P06	69,70	1582,19	3758	3434,09	0,41	0,44
C17P07	74,90	1700,23	4140	3750,02	0,43	0,47
C17P08	75,10	1704,77	4020	3648,74	0,47	0,47
C17P09	75,40	1711,58	3739	3414,84	0,60	0,47
C17P10	78,10	1772,87	4058	3677,89	0,54	0,48

Cycle/Point	mass flow %	ρl (kg/m3)	ρv (kg/m3)	hg (kJ/kg)	hl (kJ/kg)	hi (kJ/kg)
C14P01	58,64	738,50	36,93	2771,67	1270,97	1162,85
C14P03	52,37	738,58	36,90	2771,73	1270,73	1147,36
C14P04	52,24	738,41	36,96	2771,60	1271,23	1147,10
C14P05	55,26	738,35	36,97	2771,56	1271,38	1147,60
C14P06	58,94	738,29	37,00	2771,51	1271,57	1161,09
C14P08	55,49	738,70	36,86	2771,82	1270,39	1153,09
C14P09	52,77	738,40	36,96	2771,59	1271,26	1145,11
C14P10	58,63	738,64	36,88	2771,77	1270,57	1153,09
C15P01	59,11	737,01	37,42	2770,56	1275,24	1161,33
C15P02	55,44	737,15	37,37	2770,67	1274,83	1153,32
C15P03	52,13	737,18	37,36	2770,69	1274,75	1145,35
C15P04	59,50	737,05	37,40	2770,59	1275,12	1153,30
C15P05	56,36	737,08	37,39	2770,61	1275,04	1147,32
C15P06	53,93	737,12	37,38	2770,65	1274,92	1140,37
C15P08	57,06	737,07	37,40	2770,60	1275,08	1144,34
C15P09	51,90	737,16	37,37	2770,67	1274,81	1135,43
C15P10	60,23	737,00	37,42	2770,56	1275,26	1150,32
C16P01	58,74	737,97	37,10	2771,28	1272,48	1164,35
C16P02	56,07	737,99	37,09	2771,29	1272,42	1159,83
C16P03	52,83	738,04	37,08	2771,33	1272,27	1148,84
C16P04	59,50	737,95	37,11	2771,26	1272,54	1159,82
C16P05	56,04	737,98	37,10	2771,29	1272,45	1151,82
C16P06	52,47	738,04	37,08	2771,33	1272,27	1142,87
C16P07	58,30	737,94	37,11	2771,25	1272,58	1151,33
C16P08	55,81	737,98	37,10	2771,29	1272,46	1145,85
C16P09	52,54	738,04	37,08	2771,33	1272,30	1137,42
C16P10	60,24	737,92	37,11	2771,24	1272,62	1151,82
C16P11	52,19	738,23	37,01	2771,47	1271,74	1148,84
C17P02	56,49	738,19	37,03	2771,44	1271,87	1158,33
C17P03	52,57	738,25	37,01	2771,49	1271,68	1150,83
C17P04	59,51	738,10	37,06	2771,38	1272,11	1158,32
C17P05	57,36	738,16	37,04	2771,42	1271,93	1152,32
C17P06	53,69	738,20	37,02	2771,45	1271,82	1147,34
C17P07	59,14	738,13	37,05	2771,39	1272,04	1151,32
C17P08	57,43	738,16	37,04	2771,42	1271,95	1148,83
C17P09	53,41	738,20	37,02	2771,45	1271,82	1134,94
C17P10	57,97	738,14	37,04	2771,41	1271,99	1144,36

Cycle/Point	Nsub	Npch	Δ_{tsub}	Tsat inlet (ºC)	T inlet (K)	T inlet ºC
C14P01	1,37	5,02	20,79	286,49	538,85	265,70
C14P03	1,56	5,57	23,85	286,45	535,75	262,60
C14P04	1,57	6,00	23,99	286,54	535,70	262,55
C14P05	1,57	5,70	23,92	286,57	535,80	262,65
C14P06	1,40	5,38	21,26	286,61	538,50	265,35
C14P08	1,49	6,12	22,63	286,38	536,90	263,75
C14P09	1,60	6,17	24,40	286,55	535,30	262,15
C14P10	1,49	6,02	22,67	286,42	536,90	263,75
C15P01	1,42	4,90	21,89	287,29	538,55	265,40
C15P02	1,52	5,25	23,42	287,22	536,95	263,80
C15P03	1,62	5,55	25,00	287,20	535,35	262,20
C15P04	1,52	5,28	23,47	287,27	536,95	263,80
C15P05	1,60	5,56	24,66	287,25	535,75	262,60
C15P06	1,68	5,80	26,03	287,23	534,35	261,20
C15P08	1,64	5,90	25,27	287,26	535,15	262,00
C15P09	1,75	6,08	27,01	287,21	533,35	260,20
C15P10	1,56	5,76	24,10	287,30	536,35	263,20
C16P01	1,36	4,92	20,78	286,78	539,15	266,00
C16P02	1,42	5,17	21,66	286,77	538,25	265,10
C16P03	1,56	5,46	23,84	286,74	536,05	262,90
C16P04	1,42	5,32	21,69	286,79	538,25	265,10
C16P05	1,52	5,60	23,27	286,77	536,65	263,50
C16P06	1,63	5,92	25,04	286,74	534,85	261,70
C16P07	1,53	5,75	23,40	286,79	536,55	263,40
C16P08	1,60	6,03	24,47	286,77	535,45	262,30
C16P09	1,70	6,35	26,14	286,74	533,75	260,60
C16P10	1,52	5,70	23,30	286,80	536,65	263,50
C16P11	1,55	5,66	23,74	286,64	536,05	262,90
C17P02	1,43	5,22	21,86	286,66	537,95	264,80
C17P03	1,53	5,58	23,33	286,63	536,45	263,30
C17P04	1,44	5,27	21,91	286,71	537,95	264,80
C17P05	1,51	5,49	23,08	286,67	536,75	263,60
C17P06	1,57	5,82	24,05	286,65	535,75	262,60
C17P07	1,52	5,72	23,30	286,69	536,55	263,40
C17P08	1,55	5,90	23,78	286,68	536,05	262,90
C17P09	1,73	6,33	26,55	286,65	533,25	260,10
C17P10	1,61	6,08	24,69	286,68	535,15	262,00

Cycle/Point	Pinlet(bar)	Δpinlet (bar)	Δpoutlet (bar)	Δpcore (bar)	radial peak	axial peak
C14P01	70,69	0,165	0,0319	0,471	1,696	1,294
C14P03	70,64	0,127	0,0318	0,432	1,676	1,205
C14P04	70,74	0,125	0,0316	0,429	1,615	1,831
C14P05	70,77	0,143	0,0318	0,448	1,632	1,639
C14P06	70,81	0,167	0,0319	0,473	1,653	1,472
C14P08	70,58	0,146	0,0318	0,453	1,602	1,611
C14P09	70,75	0,128	0,0317	0,433	1,612	1,994
C14P10	70,61	0,169	0,0318	0,475	1,613	1,478
C15P01	71,53	0,170	0,0320	0,477	1,568	1,247
C15P02	71,45	0,148	0,0319	0,455	1,543	1,240
C15P03	71,43	0,129	0,0318	0,435	1,633	1,295
C15P04	71,50	0,175	0,0320	0,482	1,636	1,264
C15P05	71,49	0,154	0,0319	0,461	1,626	1,281
C15P06	71,46	0,139	0,0319	0,445	1,613	1,365
C15P08	71,49	0,159	0,0318	0,465	1,626	1,769
C15P09	71,44	0,126	0,0317	0,431	1,645	1,937
C15P10	71,53	0,182	0,0318	0,488	1,642	1,855
C16P01	70,98	0,162	0,0319	0,467	1,671	1,271
C16P02	70,97	0,146	0,0318	0,451	1,663	1,318
C16P03	70,94	0,127	0,0318	0,432	1,655	1,377
C16P04	71,00	0,170	0,0318	0,476	1,660	1,361
C16P05	70,98	0,148	0,0317	0,454	1,650	1,376
C16P06	70,94	0,127	0,0317	0,432	1,641	1,366
C16P07	71,00	0,165	0,0317	0,471	1,637	1,301
C16P08	70,98	0,150	0,0317	0,455	1,634	1,296
C16P09	70,95	0,130	0,0316	0,436	1,633	1,281
C16P10	71,01	0,179	0,0317	0,485	1,632	1,244
C16P11	70,84	0,125	0,0317	0,430	1,659	1,599
C17P02	70,86	0,149	0,0318	0,455	1,625	1,343
C17P03	70,83	0,126	0,0317	0,432	1,630	1,335
C17P04	70,91	0,170	0,0318	0,476	1,624	1,340
C17P05	70,88	0,156	0,0318	0,463	1,624	1,367
C17P06	70,85	0,134	0,0317	0,440	1,630	1,361
C17P07	70,90	0,170	0,0317	0,476	1,626	1,310
C17P08	70,88	0,159	0,0317	0,465	1,632	1,305
C17P09	70,86	0,134	0,0316	0,440	1,645	1,339
C17P10	70,89	0,164	0,0317	0,470	1,646	1,311

Cycle/Point	Height from bottom (cm)	Plane number	ΔP-separator (bar)	total power coefficient
C14P01	257,60	19	0,179	-9,190E-04
C14P03	198,72	15	0,171	-9,110E-04
C14P04	36,80	4	0,172	-7,580E-04
C14P05	51,52	5	0,182	-7,700E-04
C14P06	51,52	5	0,195	-7,750E-04
C14P08	51,52	5	0,184	-7,270E-04
C14P09	36,80	4	0,174	-7,380E-04
C14P10	66,24	6	0,197	-7,020E-04
C15P01	139,84	11	0,193	-9,150E-04
C15P02	169,28	13	0,167	-9,070E-04
C15P03	110,40	9	0,170	-9,050E-04
C15P04	110,40	9	0,183	-8,230E-04
C15P05	110,40	9	0,185	-8,190E-04
C15P06	66,24	6	0,177	-8,050E-04
C15P08	51,52	5	0,190	-7,040E-04
C15P09	51,52	5	0,171	-7,610E-04
C15P10	51,52	5	0,202	-6,680E-04
C16P01	51,52	5	0,179	-8,490E-04
C16P02	51,52	5	0,183	-8,430E-04
C16P03	51,52	5	0,172	-8,550E-04
C16P04	36,80	4	0,184	-7,570E-04
C16P05	36,80	4	0,185	-7,690E-04
C16P06	36,80	4	0,172	-7,830E-04
C16P07	36,80	4	0,194	-7,160E-04
C16P08	36,80	4	0,186	-7,140E-04
C16P09	36,80	4	0,174	-7,260E-04
C16P10	51,52	5	0,189	-7,020E-04
C16P11	51,52	5	0,171	-7,640E-04
C17P02	139,84	11	0,171	-8,390E-04
C17P03	139,84	11	0,158	-8,390E-04
C17P04	139,84	11	0,197	-7,820E-04
C17P05	125,12	10	0,176	-7,770E-04
C17P06	110,40	9	0,177	-7,720E-04
C17P07	110,40	9	0,185	-7,060E-04
C17P08	95,68	8	0,178	-6,980E-04
C17P09	80,96	7	0,177	-7,030E-04
C17P10	80,96	7	0,182	-6,670E-04

Cycle/Point	Xe conc	bypass flow	outlet void	axial power offset	outlet quality
C14P01	1,091E+15	380,60	0,58	1,20	0,17
C14P03	1,091E+15	309,34	0,59	0,91	0,19
C14P04	1,110E+15	306,39	0,61	0,56	0,21
C14P05	1,116E+15	342,05	0,60	0,60	0,19
C14P06	1,121E+15	384,82	0,59	0,66	0,18
C14P08	1,139E+15	348,51	0,62	0,67	0,21
C14P09	1,132E+15	313,29	0,61	0,53	0,21
C14P10	1,131E+15	387,91	0,62	0,73	0,20
C15P01	9,736E+14	389,24	0,57	1,16	0,16
C15P02	1,061E+15	350,63	0,58	1,17	0,18
C15P03	1,065E+15	313,02	0,59	1,01	0,19
C15P04	1,066E+15	397,17	0,59	1,01	0,18
C15P05	1,065E+15	362,61	0,59	0,95	0,19
C15P06	1,068E+15	333,79	0,60	0,80	0,19
C15P08	1,118E+15	371,75	0,61	0,66	0,20
C15P09	1,088E+15	308,30	0,61	0,57	0,21
C15P10	1,088E+15	409,59	0,61	0,61	0,20
C16P01	9,845E+14	376,21	0,58	0,92	0,17
C16P02	9,935E+14	347,02	0,58	0,90	0,18
C16P03	1,005E+15	309,31	0,59	0,86	0,18
C16P04	1,011E+15	390,30	0,60	0,89	0,18
C16P05	1,032E+15	351,78	0,60	0,89	0,19
C16P06	1,039E+15	310,11	0,60	0,90	0,20
C16P07	1,044E+15	381,92	0,61	0,95	0,20
C16P08	1,053E+15	354,91	0,62	0,96	0,21
C16P09	1,061E+15	316,83	0,62	0,96	0,22
C16P10	1,064E+15	404,85	0,61	0,98	0,19
C16P11	1,343E+15	305,83	0,60	0,73	0,19
C17P02	1,032E+15	352,92	0,58	1,18	0,18
C17P03	1,042E+15	307,75	0,59	1,14	0,19
C17P04	1,052E+15	389,38	0,59	1,15	0,18
C17P05	1,057E+15	365,98	0,60	1,09	0,19
C17P06	1,061E+15	323,91	0,60	1,06	0,20
C17P07	1,067E+15	389,98	0,61	1,04	0,20
C17P08	1,068E+15	371,26	0,61	1,02	0,20
C17P09	1,071E+15	324,16	0,62	0,94	0,22
C17P10	1,072E+15	380,11	0,62	0,97	0,21